

# Journal of Biomedical Optics

BiomedicalOptics.SPIEDigitalLibrary.org

## **Three-dimensional imaging and uptake of the anticancer drug combretastatin in cell spheroids and photoisomerization in gels with multiphoton excitation**

Kathrin M. Scherer  
Roger H. Bisby  
Stanley W. Botchway  
John A. Hadfield  
John W. Haycock  
Anthony W. Parker

**SPIE.**

# Three-dimensional imaging and uptake of the anticancer drug combretastatin in cell spheroids and photoisomerization in gels with multiphoton excitation

Kathrin M. Scherer,<sup>a</sup> Roger H. Bisby,<sup>b,\*</sup> Stanley W. Botchway,<sup>a</sup> John A. Hadfield,<sup>b</sup> John W. Haycock,<sup>c</sup> and Anthony W. Parker<sup>a</sup>

<sup>a</sup>Research Complex at Harwell, Central Laser Facility, STFC Rutherford Appleton Laboratory, Harwell Oxford, Didcot, OX11 0FA, United Kingdom

<sup>b</sup>University of Salford, Biomedical Research Centre, Kidscan Laboratories, Salford, Greater Manchester, M5 4WT, United Kingdom

<sup>c</sup>University of Sheffield, Kroto Research Institute, Department of Materials Science and Engineering, Broad Lane, Sheffield, S3 7HQ, United Kingdom

**Abstract.** The uptake of *E*-combretastatins, potential prodrugs of the anticancer *Z*-isomers, into multicellular spheroids has been imaged by intrinsic fluorescence in three dimensions using two-photon excited fluorescence lifetime imaging with 625-nm ultrafast femtosecond laser pulses. Uptake is initially observed at the spheroid periphery but extends to the spheroid core within 30 min. Using agarose gels as a three-dimensional model, the conversion of *Z*(trans) → *E*(cis) via two-photon photoisomerization is demonstrated and the location of this photochemical process may be precisely selected within the micron scale in all three dimensions at depths up to almost 2 mm. We discuss these results for enhanced tissue penetration at longer near-infrared wavelengths for cancer therapy and up to three-photon excitation and imaging using 930-nm laser pulses with suitable combretastatin analogs. © The Authors. Published by SPIE under a Creative Commons Attribution 3.0 Unported License. Distribution or reproduction of this work in whole or in part requires full attribution of the original publication, including its DOI. [DOI: [10.1117/1.JBO.20.7.078003](https://doi.org/10.1117/1.JBO.20.7.078003)]

Keywords: multiphoton; combretastatin; spheroid; fluorescence; imaging.

Paper 150053R received Jan. 29, 2015; accepted for publication May 28, 2015; published online Jul. 6, 2015.

## 1 Introduction

Multiphoton absorption, first proposed in 1931 by Göppert-Meyer and demonstrated with lasers in the 1960s,<sup>1,2</sup> is now widely employed in multiphoton-excited fluorescence microscopy.<sup>3,4</sup> Two- or three-photon excitations (2PE or 3PE), which have very low absorption cross sections, most readily occur at the high photon density within the femtoliter focal volume of a subpicosecond pulsed-laser excitation beam which may then be scanned across a sample to construct a fluorescence image. An important advantage in both biological imaging and phototherapy is that multiphoton excitation shifts the required wavelength to the red or near-infrared (NIR) spectral regions where light transmission in human and animal tissues is much greater than at shorter wavelengths.<sup>5</sup> However, a major concern relates to the depths that may be probed within a sample which is dependent upon several factors: light penetration and good transmission with low scattering combining to permit the necessary high peak laser power at the focus.<sup>6,7</sup> For three-dimensional (3-D) imaging of intact tissues, the choice of wavelength is important and recent work suggests that wavelengths even longer than the commonly used wavelengths ranging from ~700 to 1000 nm may be optimal.<sup>8</sup> For fixed tissues, optical clearing methods have been devised that substantially increase the sample transparency.<sup>9</sup> The issue of multiphoton excitation

has also been addressed by microscope manufacturers now offering specially designed objective lenses to optimize deep light penetration in tissues which combine specifications such as long working distance, silicon oil immersion for precise refractive index matching, chromatic aberration minimization, and high numerical aperture.

In addition to imaging studies, two-photon excitation is of increasing interest in the field of photodynamic therapy (PDT). Conventional PDT depends on photoexcitation of a drug capable of forming a triplet state, which may then either react directly with a biomolecule to form a radical species (Type I mechanism) or transfer energy to triplet ground-state dioxygen to form reactive excited singlet oxygen (Type II mechanism).<sup>10-12</sup> Type I photosensitization may involve generation of reactive oxygen species (superoxide and hydrogen peroxide) or lipid and protein radicals. In the latter instance, as with some phenothiazinium derivatives, photosensitization may be independent of oxygen.<sup>13,14</sup> This is highly desirable in practice since for photosensitization to be effective, for example, in instances where the vasculature is disrupted as in hypoxic tumor regions, Type II and some oxygen-dependent Type I mechanisms are inoperative. Two-photon excitation allows the activation wavelength to be shifted into the NIR region, improving the specificity of excitation of PDT photosensitizers while avoiding absorption by natural chromophores in the tissue, and increasing the tissue depth at which PDT may be delivered to a tumor.<sup>15-17</sup> Two-photon PDT may be achieved by using a sufficiently intense optical field (up to 800 mW) within a

\*Address all correspondence to: Roger H. Bisby, E-mail: [r.h.bisby@salford.ac.uk](mailto:r.h.bisby@salford.ac.uk)

defined region, with maximum effective depths estimated between 2 and 4 cm in tumor models and collagen gel phantoms, respectively.<sup>17</sup> It is our purpose to explore well-focussed laser beams at very much lower power levels.

Combretastatins are derivatives of natural products from the African bush willow tree, *Combretum caffrum*. They are all 1,2-diarylethenes that, as the *Z*-isomers bind strongly to tubulin, disrupt polymerization and microtubule function.<sup>18–20</sup> This results in direct toxicity to tumor cells and in the destruction of tumor vasculature through inhibition of angiogenesis. *Z*-combretastatins such as combretastatin A4 (CA4, Fig. 1) have been investigated as anticancer agents in clinical trials, and have largely proven to be effective in combination with other drugs such as carboplatin, although toxic side effects appear to be limiting their usage.<sup>21,22</sup> We have proposed that systemic toxicity of the *Z*-(cis-)isomer might be avoided by photoisomerization of the less toxic *E*-(trans-)isomer by targeted photoirradiation at a tumor site (Fig. 1).<sup>23–25</sup> While *Z*-combretastatins are non-fluorescent, the intrinsic fluorescence of *E*-combretastatins has enabled real-time monitoring of *E*-combretastatin uptake in monolayers of live mammalian cells by two-photon excitation fluorescence lifetime imaging (2PE-FLIM).<sup>23,24</sup> *E*-combretastatins have fluorescence lifetimes that are dependent on solvent polarity and viscosity and were shown to be proportional to fluorescence quantum yields. Through measurement of both fluorescence intensity and lifetimes, it was possible to evaluate intracellular concentrations. *E*-Combretastatins were found to accumulate in the cytoplasm and within intracellular lipidic structures including lipid droplets at millimolar concentrations. Once within the cell, the *E*-combretastatin (absorption  $\lambda_{\text{max}} \sim 320$  nm) may be activated by two-photon absorption at 625–630 nm and the resulting cell death demonstrated using fluorescence assays.<sup>25</sup> Both two-photon irradiation and

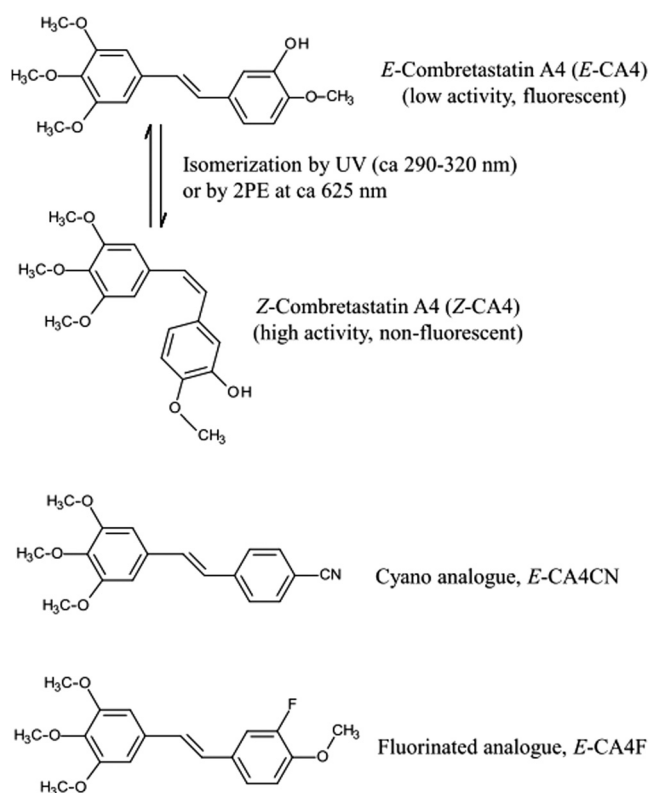


Fig. 1 Structures of the compounds used in this work.

fluorescent assays using confocal imaging may be performed using a single adapted microscope system.<sup>26</sup> The present report moves our previous work with combretastatins in monolayer cell cultures into 3-D model systems to demonstrate prodrug uptake and activation at depth within a model tissue structure. It is widely considered that tumor spheroids consisting of an assembly of several thousand cells offer more realistic tissue models<sup>27–29</sup> and are, therefore, used here to study the intracellular uptake of fluorescent *E*-combretastatins in three dimensions over time.

Thick agarose gels are used as a scattering 3-D model to demonstrate the *Z* → *E*- combretastatin photoisomerization by two-photon excitation at increasing depth with highly localized specificity. Previously, we established ~630 nm excitation to be an effective wavelength to achieve photoisomerization of combretastatins, but deep tissue penetration of the excitation light is best achieved using wavelengths even further shifted toward the NIR (>800 nm). Hence, experiments in solution were also carried out to investigate the potential of three-photon isomerization and activation of an *E*-combretastatin at these longer wavelengths of between 800 and 1000 nm where there is less scattering and where interference from melanin absorption is also reduced.

## 2 Materials and Methods

### 2.1 Cell Culture and Maintenance

C8161 human melanoma cells were a gift from Meyskens (University of California, Irvine) and were established from abdominal wall metastasis from a menopausal woman with recurrent malignant melanoma.<sup>30</sup> Human metastatic breast cancer MDA231 cells were obtained from Currell's group at the Queen's Belfast University. C8161 melanoma cells were routinely cultured in T75 tissue culture flasks using phenol-red free minimum essential medium (MEM) supplemented with 10% FBS, 100 units/mL penicillin, 100 mg/mL streptomycin and L-glutamine (2 mM). MDA 231 cells were maintained in phenol-red free DMEM (high glucose) containing the same supplements. The cells were stored under a humidified atmosphere at 37°C with 5% CO<sub>2</sub>. All cell culture materials [fetal bovine serum (FBS)], penicillin, streptomycin, L-glutamine, phosphate buffered saline (PBS, 1×), 0.5% trypsin-EDTA (10×), MEM and Dulbecco's modified Eagle's medium (DMEM) were purchased from Gibco®. Glass-bottom culture dishes (35 mm diameter, No. 1.5, uncoated,  $\gamma$ -irradiated) were obtained from MatTek Corporation, USA, and sterile 96-well round-bottom plates were purchased from BD Falcon. Agarose powder (99%) for multiwell-plate coating was purchased from Sigma-Aldrich.

### 2.2 Growth of Multicellular C8161 and MDA Spheroids

Multicellular spheroids from C8161 and MDA 231 cells were grown in round-bottom 96-well plates coated with sterile agarose gel 1.5% in PBS (100  $\mu$ L/well). The agarose gel was left to set for 1.5 h at room temperature in a sterile environment prior to cell seeding. C8161 or MDA 231 cell suspensions (100  $\mu$ L), respectively, with concentrations of  $10 \times 10^4$  cells/mL were added to each well and the wells were topped up with an extra 100  $\mu$ L of the corresponding complete media. The 96-well plates were stored for 3 to 7 days in a humidified incubator

at 37°C with 5% CO<sub>2</sub> to allow spheroid formation (normally visible after 24 to 48 h). No cells were added to the outer wells of the 96-well plates since they are prone to evaporation of cell culture media. Instead, they were filled with PBS (200 μL) to prevent evaporation of culture media from the edges. After 3 to 7 days, multicellular spheroids with average diameters of ~200 to 500 μm were harvested and carefully transferred from their well onto MatTek glass-bottom culture dishes and immersed in FITC-dextran (final concentration 0.25 mg/mL, Sigma-Aldrich) containing medium for microscopic examination.

### 2.3 Confocal and Two-Photon Fluorescence Lifetime Imaging of Multicellular Spheroids

Confocal and multiphoton fluorescence lifetime imaging of MDA 231 and C8161 multicellular spheroids was carried out using an inverted Nikon TE2000-U microscope attached to a Nikon C2 scanning unit. The imaging was carried out using a Nikon Plan Apo VC 60× water immersion objective (N.A. 1.2, WD 0.31 to 0.28 mm) or Nikon Plan Apo Lambda 20× air objective (N.A. 0.75, WD 1 mm). Experiments with a single spheroid of each cell type were performed in triplicate and produced similar results. For two-photon excitation and fluorescence lifetime imaging microscopy via time-correlated single-photon counting at ~625 nm, a laser beam (from a Ti-sapphire laser producing 180 fs pulses at 76 MHz, pumping a Mira OPO) was directed through the confocal scan head onto the sample. The microscope setup has been described in detail elsewhere.<sup>26</sup> Fluorescence lifetimes were measured using the time-correlated single-photon counting method using a R3809U photomultiplier (Hamamatsu) and a Becker and Hickl SPC 830 module. For FLIM studies of *E*-combretastatin fluorescence, a combination of Comar 400IU25 and BG3 filters were used in front of the photomultiplier. FLIM data were analyzed using the SPCImage software package (Becker and Hickl). *E*-Combretastatin concentrations ( $C_s$ ) in tumor spheroids were calculated from the fluorescence intensity ( $I_s$ , counts/pixel) and lifetime ( $\tau_s$ ) using the relationship  $C_s = (I_s \cdot C_r \cdot \tau_s) / (I_r \cdot \tau_r)$ , where the standard reference values ( $C_r$ ,  $I_r$ ,  $\tau_r$ ) were obtained using solutions of *E*-combretastatin in dimethyl sulfoxide. For imaging cells using two-photon excitation, laser powers were <1 mW and the laser scanned with a typical dwell time of 1.68 μs and a pixel size of 1.4 μm. *E*- and *Z*-isomers of combretastatin CA4 (CA4), a fluorinated analog (CA4F), and a 4-cyano analog (4-[2-(3,4,5-trimethoxyphenyl)vinyl]benzonitrile, CA4CN) were prepared as previously described<sup>14,15</sup> and structures are shown in Fig. 1.

### 2.4 Isomerization in Agarose Gels

An aliquot (50 μL) of agarose (1% in PBS) containing *Z*-CA4F, *Z*-CA4 or *Z*-CA4CN (1 mM), respectively, was pipetted into a μ-Slide Angiogenesis (Ibidi®) microwell. After setting, the gel was overlaid with PBS (10 μL) to prevent it from drying out during the experiment. At this concentration, the *Z*-combretastatins form microcrystals in the gel. Irradiations were performed using the same inverted microscope system as described above, but in addition to the two microscope objectives described in the previous paragraph, irradiations also used a Nikon CF175 Apo 25 × W MP (NA 1.10 WD 2.0, a kind loan from Nikon United Kingdom) water dipping objective, specifically designed for multiphoton applications. X-Y planes of the gel (83 × 112 μm<sup>2</sup>) were irradiated with the laser beam (625 nm, 8.4 mW average

power, total time 150 s, pixel dwell time 60 μs) focused at increasing height (*Z*-dimension) into the gel. Following the irradiations, a *Z*-stacked image of the gel was acquired using the 625-nm laser beam attenuated to 0.8 mW (500 μm<sup>2</sup> XY field, 75 s accumulation 1.68 μs pixel dwell time) with emission detected with the blue channel of the confocal accessory. Maximum projection of the irradiated *Z*-stack image was analyzed using ImageJ software.

### 2.5 Multiphoton Excitation Spectra of *E*-CA4CN

Multiphoton excited fluorescence spectra were recorded by exciting a solution of *E*-CA4CN in dimethylsulfoxide (DMSO) (10 mM) at wavelengths between 800 to 960 nm using the output from the femtosecond pulsed Ti-sapphire laser at laser powers ranging from ~0.1 to 6 mW at the sample. The excitation light was delivered to the sample through the Nikon Plan Apo VC 60× water immersion objective (N.A. 1.2, WD 0.31 to 0.28 mm) without scanning the laser beam. The spectrograph (Acton 275) for the measurement of two- and three-photon excited emission spectra was calibrated using a Hg-lamp. Spectral detection was achieved using an Andor charge-coupled device camera.

## 3 Results and Discussion

### 3.1 Imaging and *E*-combretastatin Uptake in Cell Spheroids.

Tumor cell spheroids are widely considered as a closer model to tissues than cell monolayers since they are 3-D structures and display some of the characteristics of solid tumors such as low central oxygen tension and a necrotic central core.<sup>27–29</sup> They are suitable for imaging studies to an extent, but previous studies noted difficulty in resolving complete spheroid structures due to low light transmission and high scattering by the spheroid equator.<sup>28,29,31</sup> Figure 2 shows the orthogonal views of a negative image of a melanoma C8161 cell spheroid suspended in a FITC-dextran solution reconstructed from confocal *Z*-scans, together with depth-resolved images. The negative image of the spheroid, with a diameter of ~250 μm (volume 8.2 × 10<sup>6</sup> μm<sup>3</sup> and estimated to contain ca. 16,000 cells based on a single cell diameter of 10 μm (volume 520 μm<sup>3</sup>), shows that an overall approximately hemispherical shape of the lower half of the spheroid is clearly resolved in the fluorescent suspending medium by the inverted microscope by imaging of sections upward from the cover slip toward the equator (to ~100 μm). However, the top half of the spheroid is essentially represented as a shadow due to absorption and scattering by the lower half of the spheroid. This is very similar to results of cell spheroid imaging previously reported.<sup>31</sup> However, despite this issue, our results show (Fig. 3) that 3-D investigations of drug uptake are feasible at depths up to 80–100 μm into the structure using two-photon excited confocal imaging.

*E*-combretastatins are fluorescent with fluorescence lifetimes that are dependent on their environment, including local viscosity that affects the isomerization rate.<sup>23,24</sup> Uptake and distribution of *E*-combretastatin A4 (*E*-CA4) in cell monolayers of melanoma C8161 cells has been studied by real-time FLIM. As in other cells previously studied,<sup>23</sup> uptake of *E*-combretastatin is fast ( $t_{1/2} < 2$  min) and the compound is mainly located at intracellular loci that have been identified as membranes and lipid droplets.<sup>23</sup> The fluorescence lifetime of the intracellular

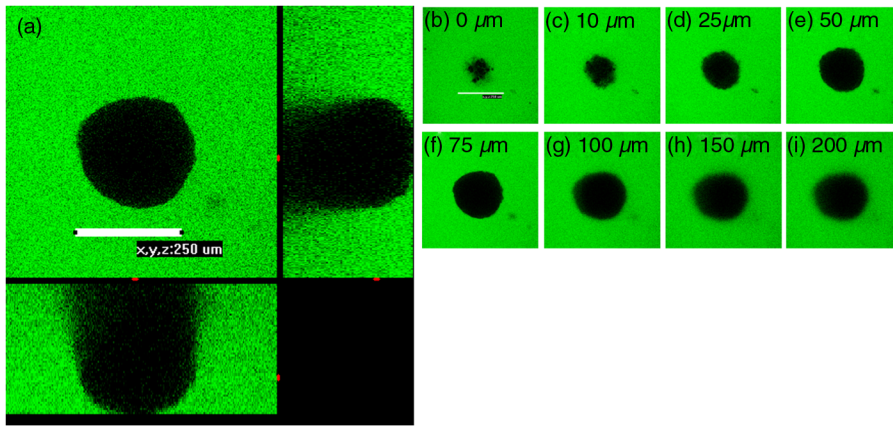


**Fig. 2** Orthogonal views (a) of a melanoma C8161 cell spheroid suspended in a solution of FITC-dextran (0.25 mg/ml, MW = 40,000 Da), producing a negative image of the spheroid (all views at the same scale). The views are reconstructed from a Z-stack of confocal images with excitation of FITC-dextran at 488 nm. Images (b) to (i) show defined planes of spheroid at the indicated distances from the coverslip.

fluorescence has a distribution that peaks at ca. 1000 ps, longer than in solution (e.g., 280 ps in ethanol and 860 ps in hexane), resulting from a viscous lipidic environment.

Results from FLIM of *E*-CA4 uptake in C8161 spheroids are shown in Fig. 3. The full depth of the spheroid cannot be imaged as noted above, and the observed images of *E*-combretastatin fluorescence after uptake over a range of imaging depth [Figs. 3(b1) to 3(b7)] show an approximate 60% decline in intensity at 75  $\mu\text{m}$  compared with 25  $\mu\text{m}$  [Fig. 3(d)]. To observe the kinetics of uptake, an optical section at 75  $\mu\text{m}$  into the

spheroid (i.e., above the cover slip) was selected and imaged using the pseudoconfocal nature of two-photon excitation. Images at selected time intervals after addition of *E*-CA4 (25  $\mu\text{M}$ ) to the medium are shown in Figs. 3(a1) to 3(a12), and reveal initial rapid uptake into the peripheral cells in this section at a rate similar to that in monolayers. After about 10-min incubation, there is significant movement of *E*-CA4 into the center of the spheroid image plane. Finally, in the last image, Fig. 3(a12), the drug appears relatively evenly distributed within this spheroid section. Similar results were obtained for *E*-CA4F

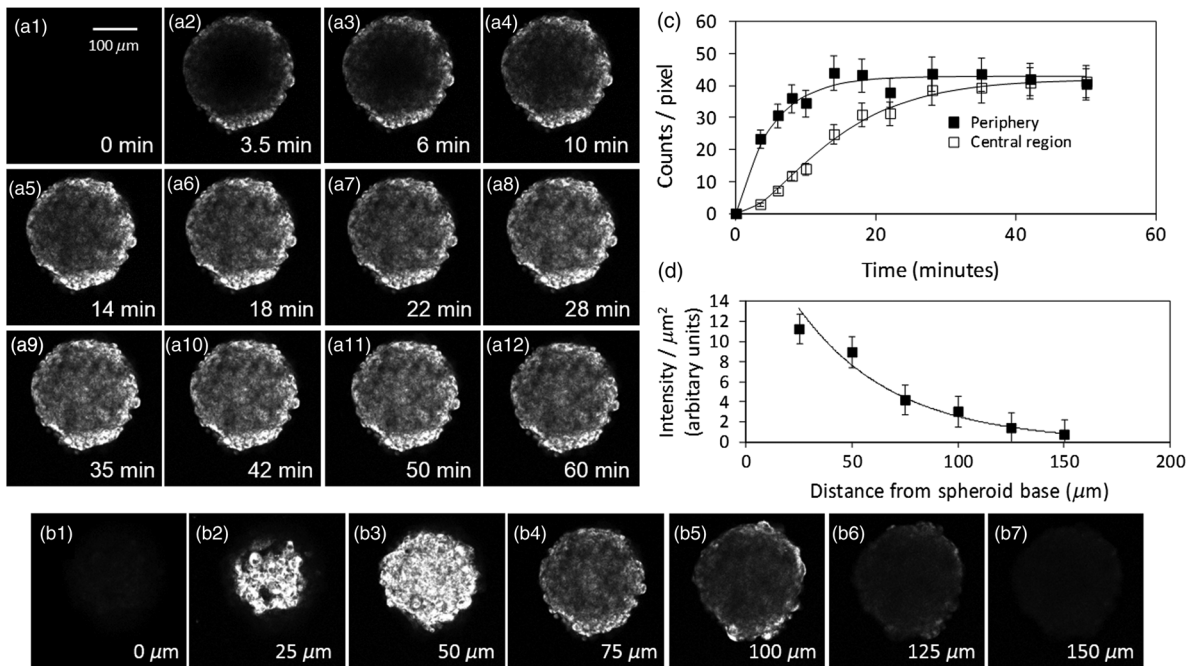


**Fig. 3** Uptake of *E*-CA4 into a C8161 melanoma cell spheroid at 20°C measured using fluorescence lifetime microscopy (FLIM) with two-photon excitation at 625 nm. (a1)–(a12) A plane 75  $\mu\text{m}$  up from the base of the spheroid using intrinsic *E*-CA4 fluorescence at the indicated times after addition of *E*-CA4 (25  $\mu\text{M}$ ) to the suspending medium. (b1)–(b7) Planes at the indicated depths within the spheroid after 60-min incubation with *E*-CA4 (25  $\mu\text{M}$ ). (c) The time course of *E*-CA4 fluorescence increase at the spheroid periphery and central region, and (d) the corresponding measured average fluorescence intensities (counts/ $\mu\text{m}^2$ ) versus imaging depth. Images were obtained with a 20 $\times$  air objective. Errors are based on an average of those from the statistics of photon counting and the measured variation in intensities of binned columns in the images.

uptake into spheroids of MDA231 cells. Figure 3(c) shows that intensity ( $I_{\text{edge}}$ ) representing uptake of the *E*-CA4 from the surrounding medium into the cells of the outer edge region (thickness of  $44\ \mu\text{m}$  from the spheroid outer surface) follows first-order kinetics [Eq. (1)] with a half-life of 3.5 min ( $k = 0.2\ \text{min}^{-1}$ ). The data for drug accumulation into the center region (from the spheroid center to within  $45\ \mu\text{m}$  of the surface) of the imaged slice of the spheroid show a sigmoidal shape that is characteristic of the accumulation of a product in a series of sequential reactions (i.e.,  $A \rightarrow B \rightarrow C$  where *A* might represent drug in the suspending medium, *B* is the drug in the peripheral cell layer, and *C* is the drug at the spheroid center). Accordingly, the curve in Fig. 3(c) for increase in intensity of fluorescence in the central region ( $I_{\text{centre}}$ ) shows a good fit to the appropriate kinetics<sup>32</sup> for species *C* [Eq. (2)] with similar, though by necessity nonidentical, first-order rate constants  $k_1 \cong k_2 \cong 0.15\ \text{min}^{-1}$ . After drug uptake was completed, a series of images in the *Z*-dimension were recorded using *E*-CA4 fluorescence and are shown in Figs. 3(b1) to 3(b7). These show clearly resolved cellular distribution at the base of the spheroid [Figs. 3(b2) at  $25\ \mu\text{m}$ ], but reveal increasing lack of imaging capability toward the spheroid equator in the same manner as was revealed in the FITC-dextrin images in Fig. 2.

$$I_{\text{edge}} = I_{\text{max}}[1 - \exp(-kt)], \quad (1)$$

$$I_{\text{centre}} = I_{\text{max}} \left\{ 1 + \frac{1}{(k_1 - k_2)} [k_2 \exp(-k_1 t) - k_1 \exp(-k_2 t)] \right\}. \quad (2)$$

These two-photon excitation FLIM results obtained with a standard confocal microscope system with a Nikon 20 $\times$  (NA 0.75, WD, 1 mm) air objective show the ability to image detail

in spheroids at depths only up to about  $100\ \mu\text{m}$ , possibly due to scattering of the violet wavelength (380–400 nm) of *E*-CA4 fluorescence. In addition to the kinetics of *E*-combretastatin uptake into the spheroid discussed above, it is also evident from the images in Fig. 3 [e.g., (b4) to (b6)] that the brightness of the image at the spheroid perimeter is greater than in the central regions. This reflects the lower optical attenuation of excitation and fluorescence by the lower cell thickness at the spheroid periphery compared with that closer to the spheroid center.

In our application of two-photon-induced isomerization of combretastatins applied to tumor phototherapy, there is clearly the need to obtain effective deeper tissue penetration. It is worth noting that two-photon excitation phototherapy requires only light delivery to the target, whereas multiphoton imaging needs both delivery and collection of photons. Thus, the multiphoton activation process in the red to NIR region is likely to be effective at greater depths than that reported here.

The concentrations of *E*-CA4 in the spheroid shown in Fig. 3 have been calculated using FLIM data and an example is shown in Fig. 4(a) using the image after 10 min incubation shown in Fig. 3(a4). The FLIM image [Fig. 4(b)] and the fluorescence lifetime distribution [Fig. 4(d)] show a fairly narrow distribution of lifetimes peaking at 1014 ps, and a good fit to a single exponential fluorescence decay is evident at an individual location (averaged over 4 pixels) in the image [Fig. 4(c)]. The concentrations at each pixel in the image are calculated as previously described for cell monolayers,<sup>23</sup> using a series of *E*-CA4 solutions in DMSO for intensity calibration and making an adjustment for lifetime in the spheroid image, since for *E*-CA4, the fluorescence quantum yield is directly proportional to lifetime.<sup>23</sup> The concentration image [Fig. 4(a)] shows that intracellular concentrations of *E*-CA4 reach values of 10–20 mM compared with the  $25\ \mu\text{M}$  concentration of *E*-CA4 in the added medium. The concentrations are also reflected in the relative color

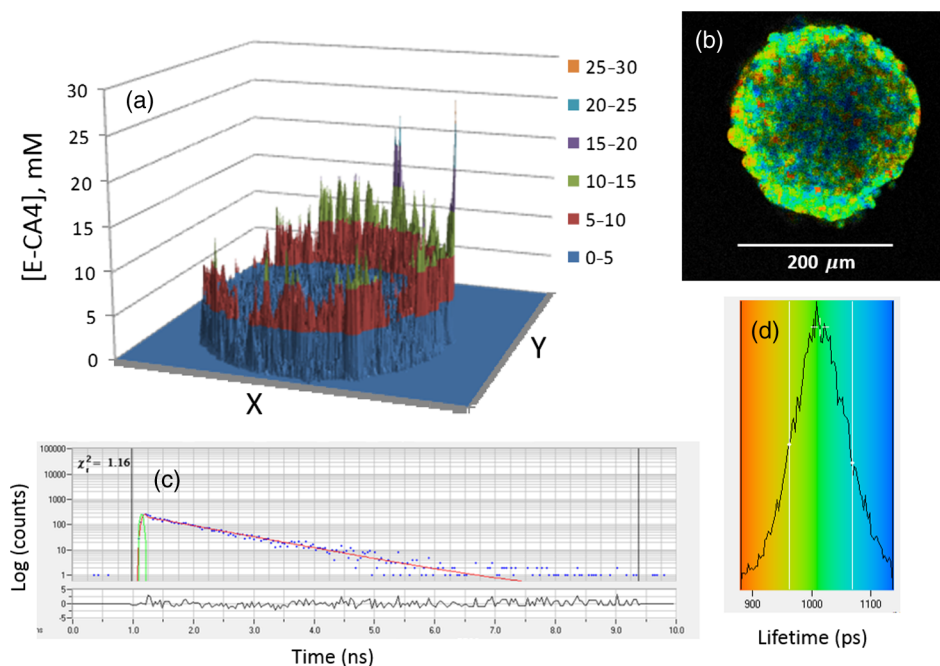


**Fig. 4** Concentration profiles for *E*-CA4 within a C8161 melanoma cell spheroid obtained by FLIM. (a) Concentration map for *E*-CA4 in the spheroid after 10 min incubation based on the image in Fig. 3(a4). (b) FLIM image of the imaged plane of the spheroid. (c) Fluorescence decay trace for *E*-CA4 within the spheroid showing a good single exponential. (d) Fluorescence lifetime distribution for the image shown in (b). The dimensions of the field (*X*, *Y*) in A and B are  $350\ \mu\text{m}^2$ .

brightnesses of the lifetime image [Fig. 4(b)]. This high extent of accumulation of *E*-CA4 into cells was previously observed in cell monolayers and attributed to the high lipophilicity of the compound.<sup>23</sup>

### 3.2 Combretastatin Isomerization in Agarose Gels

The problem of obtaining a tightly focused laser beam at depth within tissues depends on light scatter and absorption within the medium. However, recently improved lens designs offer considerable improvements and commercial developments have led to new lenses that are specifically designed to meet the demands of multiphoton microscopy. In order to compare effective penetration depths for our photochemical combretastatin isomerization, we have studied agarose gels containing the nonfluorescent *Z*-combretastatin isomer. While this is the reverse reaction of that required for combretastatin activation with regard to targeted cancer therapy, it allows visualization of the isomerization reaction by formation of the readily detected fluorescence of the resulting *E*-isomer.

An aqueous solution containing agarose (1%) and *Z*-CA4 (1 mM) produced a scattering gel, in which the combretastatin appears to have precipitated. The gel was placed into an Ibidi  $\mu$ -Slide Angiogenesis on the inverted confocal fluorescence microscope and could be irradiated from below with the pulsed (200 fs) laser beam at 625 nm in order to attempt photoisomerization by two-photon absorption. The gel was irradiated by focusing the laser at a selected focal plane and then raster scanning over a central  $83 \times 112 \mu\text{m}^2$  area of the available field of view. This process was repeated in the same gel sample at increasing depths in the sample. A *Z*-stack image of the gel *in situ* using the same laser wavelength at reduced power then recorded fluorescence from any *E*-combretastatin resulting from two-photon isomerization of the *Z*-combretastatin. Figure 5 shows the results obtained using the Nikon CF175 Apo 25 $\times$  W MP (NA 1.10 WD 2.0) water dipping objective, specifically designed for multiphoton applications. The *Z*-scan image

[Fig. 5(a)] clearly reveals the irradiated planes imaged by fluorescence of an irradiation product. It is notable that photoisomerization may be initiated and imaged at depths of up to  $1700 \mu\text{m}$  within the gel, although the efficiency of activation falls with distance [Fig. 5(b)]. The particulate nature of the *Z*-CA4 precipitate within the gel is revealed by the gray-scale image of the irradiated area at a depth of  $700 \mu\text{m}$  within the gel [Fig. 5(c)]. The ability of this lens to perform at working distances approaching 2 mm shows that combretastatin activation may be achievable within tissues. Comparable experiments with the other available lenses, such as the Nikon 60 $\times$  water immersion objective (N.A. 1.2), which we have routinely used in previous studies of cell monolayers<sup>23,24</sup> demonstrate photoisomerization is limited to much lower penetration depths typically of around  $200 \mu\text{m}$  for the 60 $\times$  water immersion objective, and up to around  $500 \mu\text{m}$  with the Nikon 20 $\times$  air objective.

### 3.3 Comparison of Two- and Three-Photon Absorptions by Combretastatins

The efficiency for combretastatin drug activation by *E*  $\rightarrow$  *Z* photoisomerization will depend on the effects of wavelength on optical tissue penetration and the extent of light absorption, the latter being determined by the absorption cross section. Two-photon absorption cross sections for *E*-CA4F are highly wavelength dependent and increase as the excitation wavelength decreases from 630 to 560 nm.<sup>14</sup> We have found that cyano-substituted combretastatins have greatly enhanced two-photon absorption cross sections in this wavelength region presumably due to the charge transfer nature of the electronic state by virtue of the electron withdrawing cyano-group.<sup>33,34</sup> One such compound that is accumulated in cells in the same way as *E*-CA4 is *E*-CA4CN, a B-ring 4-cyano substituted combretastatin analog (Fig. 1).<sup>24</sup> Further access to the tissue optical window at  $>650 \text{ nm}$  is made possible via possible three-photon absorption. This was explored for *E*-CA4CN which has a one-photon absorption maximum in DMSO at 344 nm thus offering the

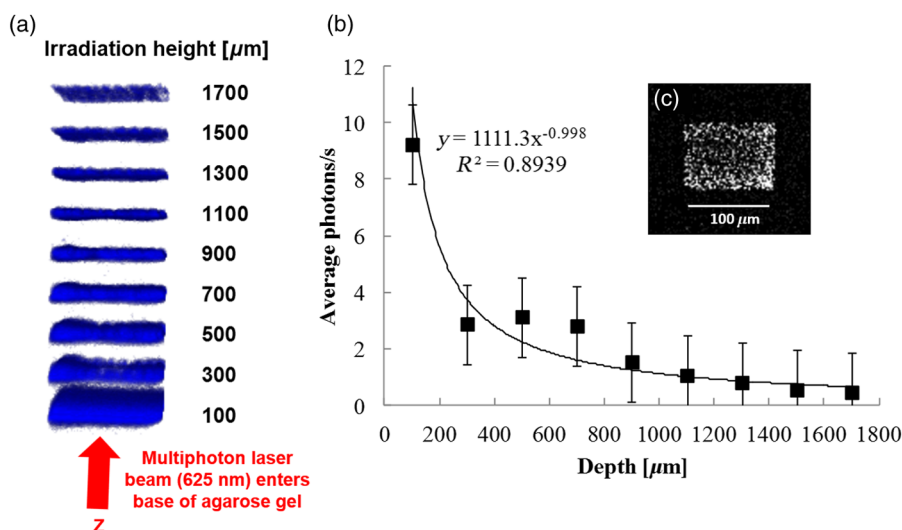


**Fig. 5** Images of an agarose gel [1% in phosphate buffered saline (PBS)] containing *Z*-CA4 (1 mM) showing fluorescence in planes irradiated with a rastered focused laser beam at 625 nm. (a) 3-D projection of fluorescence intensity revealing irradiated planes within the gel. (b) Plot of integrated fluorescence intensity versus irradiation depth in the gel. (c) A 2-D image of the fluorescence at  $700 \mu\text{m}$  into the gel. Recorded using a Nikon 25 $\times$ , 1.1 NA, 2 mm working distance multiphoton objective. Errors are based on an average of those from the statistics of photon counting and the measured variation in intensities of binned columns in the images.

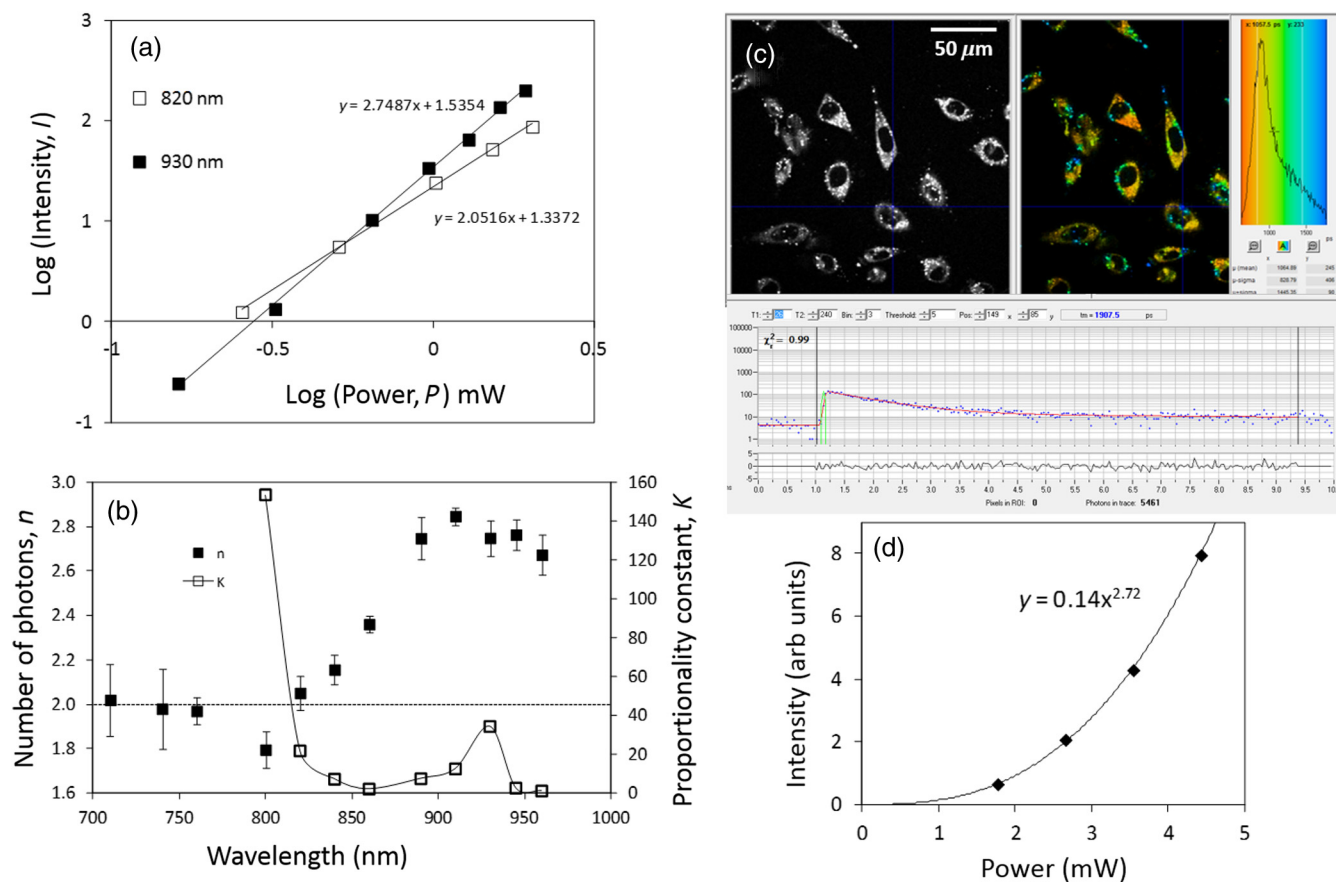


**Fig. 6** Multiphoton excited fluorescence from *E*-CA4CN. (a) Log–log plots of fluorescence intensity versus laser power at 820 nm (square) and 930 nm (filled square) for *E*-CNCA4 (10 mM) in dimethyl sulfoxide. (b) Effect of wavelength on the power dependency [ $n$ , Eq. (3), left scale filled square] and proportionality constant [ $K$ , Eq. (3), arbitrary units, right hand scale square]. (c) FLIM images of *E*-CA4CN in HeLa cells obtained 60 min after addition of *E*-CA4CN (50  $\mu\text{M}$ ) to the medium and on excitation at 930 nm (1.8 mW). (d) Plot of integrated intensity in FLIM image (c) versus excitation power at 930 nm.

possibility of three-photon absorption in the region of 900–1000 nm which is further into the tissue window than the region of 625 nm explored for two-photon excitation as above, with the results shown in Fig. 6. The power ( $P$ ) dependence for fluorescence intensity ( $I$ ) in processes involving  $n$  photons is expected to follow Eq. (3), where  $K$  is the proportionality constant

$$I = KP^n. \quad (3)$$

Log–log plots of fluorescence intensity versus laser power have slopes of  $2.05 \pm 0.08$  and  $2.75 \pm 0.08$  at 820 and 930 nm, respectively [Fig. 6(a)], indicating the two- and three-photon processes, respectively. The three-photon process appears to dominate at wavelengths  $>900$  nm [Fig. 6(b)]. The much higher cross section for two-photon absorption compared with that for the three-photon process is probably the reason why a value of 3 is not reached at the longer wavelengths. The relative efficiency of excitation at the two wavelengths was estimated from the value of  $K$  in Eq. (3) irrespective of the value of  $n$ , and is plotted versus wavelength in Fig. 6(b). This shows a surprisingly sharp absorption peak in the three-photon cross section at 930 nm, considering that the one-photon spectrum has a full width at half maximum of ca. 60 nm, and indicates the need for careful measurement of multiphoton spectra. Although the efficiency of three-photon absorption is considerably less than for two

photons, imaging of *E*-CA4CN within cells is possible at moderate laser powers as demonstrated by the FLIM data in Fig. 6(c) using 1.8 mW of laser power at the sample at 930 nm. The integrated intensity of the image versus laser power shows a value of  $n = 2.72$  similar to that obtained in solution [Fig. 6(d)] at this wavelength. The FLIM images show *E*-CA4CN to be concentrated within the cytoplasmic region with an intracellular peak fluorescence lifetime of *E*-CA4CN of 0.80 ns ( $\chi^2 = 1.35$ ), which was shorter than the lifetimes found for the other *E*-combretastatins, but corresponds well to the fluorescence lifetime of *E*-CA4CN measured in ethylene glycol solution (0.84 ns). The shorter fluorescence lifetimes of *E*-CA4CN in nonpolar lipid droplets are in accordance with the finding that fluorescence lifetimes in the nonpolar solvents cyclohexane and hexane were also short compared to the lifetimes of all other *E*-combretastatin derivatives within nonpolar environments.<sup>34</sup>

## 4 Conclusions

Real-time imaging of *E*-combretastatin uptake in live mammalian cell spheroids has been demonstrated by multiphoton-excited fluorescence microscopy. Although only approximately half of the spheroid may be effectively imaged because of photon scatter and absorption, particularly in the ultraviolet spectral region where more scattering ( $\propto \lambda^{-4}$ ) is expected, the method is able to probe sections close to the spheroid equator and

demonstrate rapid initial uptake at the spheroid periphery followed by diffusion to the spheroid interior. Equilibration of *E*-combretastatin throughout the spheroid is effectively completed within 30 min and this is faster than has been observed for Cy-3 labeled aptamer or peptide in C6 cell spheroids.<sup>35</sup> Our approach has the advantage of tracking uptake by intrinsic fluorescence without the need for a conjugated fluorescence probe and permits imaging in live cell spheroids rather than using fixed specimens. Although the difference in uptake into a spheroid may be accounted for by the difference in molecular size, it may be noted that doxorubicin penetration into spheroids is also slow with a half-life of hours and penetration of derivatized quantum dots showed a strong dependence on charge.<sup>29</sup> Confocal microscopy has also been used to study small inhibitory RNA uptake in multicellular spheroids and revealed penetration only into the spheroid periphery.<sup>36</sup> The inability to image a complete spheroid by multiphoton and confocal microscopy has been previously noted<sup>29,31</sup> and light sheet microscopy appears to provide superior imaging capability for spheroids.<sup>37</sup>

Various 3-D models for PDT have been investigated including tumor spheroids, tumor nodules, and scaffold-based cultures.<sup>12</sup> Using spheroids, Foster et al.<sup>38</sup> found evidence that using the singlet oxygen generating photosensitizer photofrin resulted in substantial oxygen depletion and the formation of hypoxic regions in the spheroid center where oxygen diffusion is limited and led to enhanced survival of cells in this region after treatment. PDT involving oxygen-dependent sensitizer mechanisms will, therefore, potentially limit the application of PDT to solid tumors which likewise possess hypoxic regions. However, one photosensitizer, EtNBS (5-ethylamino-9-diethylaminobenzo[a]phenothiazinium chloride) has been found<sup>39–41</sup> to effectively penetrate into a 3-D tumor nodule model (diameter 200  $\mu\text{m}$ ) and spheroids, and kills hypoxic cells at the core through an oxygen-independent Type I radical mechanism.<sup>39</sup> Similarly, *E*-combretastatins are shown here to readily diffuse to the central regions of similar diameter tumor spheroids and since their photoisomerization and activation to the *Z*-isomer is an oxygen independent process, they should be effective within hypoxic regions of cell models and tumors. We have attempted to study cell killing within small defined regions of tumor spheroids following treatment using the same approach as in our previous successful work<sup>25</sup> with cell monolayers. These experiments involved *E*-combretastatin uptake into the spheroid, photoirradiation (typically of a  $150 \times 50 \times 10 \mu\text{m}^3$  volume at 50  $\mu\text{m}$  height into the spheroid), and incubation for 24 to 48 h followed by apoptotic cell labeling. Although we have observed a lawn of dead cells at the base of the spheroid following irradiation, we were unable to identify a region of dead or apoptotic cells corresponding to the irradiated region within the spheroid. It may be that with the spheroid environment, dead cells are replaced within the 24–48 h incubation by live cells from the regions that border the irradiated section on at least three sides. Further studies are required with an alternative more rapid assay to identify apoptosis in 3-D structures.

Although *Z*-combretastatins are primarily antivascular agents, their ability to induce apoptosis suggests that oxygen independent photoactivation of *E*-combretastatins should be active against hypoxic cells within the center of spheroids and tumor cores.<sup>37,38</sup> This is seen as a potential major benefit in external treatment of accessible tumors or in combination with surgical resection for other sites such as the bile duct<sup>42</sup> or skin. For example, PDT has been trialed for treating

melanoma, but outcomes show it to be generally resistant. Problems include optical interference by melanin pigmentation, melanin antioxidant properties, and apoptotic pathway defects.<sup>43</sup> To overcome this, photosensitizers that absorb in the NIR spectral region (700–800 nm) have been considered together with interventions for reducing melanin pigmentation and immunotherapy approaches. Although localized *E*  $\rightarrow$  *Z* activation and toxicity of combretastatins could not be directly determined in spheroids at this stage, it was possible to demonstrate two-photon *Z*  $\rightarrow$  *E* isomerization at depth within agarose gels. This suggests that *E*-combretastatin activation within tissues for tumor phototherapy is an achievable objective. Finally, it has been shown that for suitable *E*-combretastatin molecules with optimized cross sections, the two-photon imaging and activation may be extended to the three-photon regime within the potential benefits of extending the activation wavelength further into the NIR region. These findings make *E*-combretastatins good candidates for targeted cancer therapy and our results demonstrate the need for further studies into their potential use as phototherapeutic agents. By affording localized delivery of the active drug to the tumor site, the systemic toxicity that currently limits the clinical use of *Z*-combretastatins<sup>44</sup> might be avoided.

### Acknowledgments

The authors thank STFC for providing funding (Grant No. ST/K001914/1) and access to laser laboratories at the Central Laser Facility, Rutherford Appleton Laboratory and Laserlab, EC-GA 284464 for further support. We gratefully acknowledge Nikon UK for the loan of the multiphoton objective. The research materials supporting this publication may be accessed by contacting the corresponding author, R.H.B.

### References

1. S. Singh and L. T. Bradley, "Three-photon absorption in naphthalene crystals by laser excitation," *Phys. Rev. Lett.* **12**(22), 612–614 (1964).
2. B. R. Masters and P. T. C. So, "Antecedents of two-photon excitation laser scanning microscopy," *Microsc. Res. Tech.* **63**(1), 3–11 (2004).
3. K. König, "Multiphoton microscopy in life sciences," *J. Microsc.* **200**(2), 83–104 (2000).
4. A. Ustione and D. W. Piston, "A simple introduction to multiphoton microscopy," *J. Microsc.* **243**(3), 221–226 (2011).
5. C. Wang et al., "Extension of imaging depth in two-photon fluorescence microscopy using a long-wavelength high-pulse-energy femtosecond laser source," *J. Microsc.* **243**(2), 179–183 (2011).
6. R. Weissleder and V. Ntziachristos, "Shedding light onto live molecular targets," *Nat. Med.* **9**(1), 123–128 (2003).
7. F. O. Fährbach et al., "Light-sheet microscopy in thick media using scanned Bessel beams and two-photon fluorescence excitation," *Opt. Express* **21**(11), 13824 (2013).
8. N. G. Horton et al., "In vivo three-photon microscopy of subcortical structures within an intact mouse brain," *Nat. Photonics* **7**(3), 205–209 (2013).
9. H. Hama et al., "Scale: a chemical approach for fluorescence imaging and reconstruction of transparent mouse brain," *Nat. Neurosci.* **14**(11), 1481–1488 (2011).
10. B. W. Henderson and T. J. Dougherty, "How does photodynamic therapy work?," *Photochem. Photobiol.* **55**(1), 145–157 (1992).
11. B. C. Wilson and M. S. Patterson, "The physics, biophysics and technology of photodynamic therapy," *Phys. Biol. Med.* **53**(9), R61–R109 (2008).
12. M. Alemany-Ribes et al., "Why not introducing the third dimension in photodynamic therapy research?" *J. Anal. Bioanal. Tech.* S1:004 (2013).

13. L. Cincotta et al., "Novel photodynamic effects of a benzophenothiazine on two different murine sarcomas," *Cancer Res.* **54**(5), 1249–1258 (1994).
14. C. L. Evans et al., "Killing hypoxic cell populations in a 3D tumor model with EtNBS-PDT," *PLoS ONE* **6**(8), e23434 (2011).
15. T. Luo, B. C. Wilson, and Q.-B. Lu, "Evaluation of one- and two-photon activated photodynamic therapy with pyropheophorbide-a methyl ester in human cervical, lung and ovarian cancer cells," *J. Photochem. Photobiol. B* **132**, 102–110 (2014).
16. C. Fowley et al., "Extending the tissue penetration capability of conventional photosensitisers: a carbon quantum dot–protoporphyrin IX conjugate for use in two-photon excited photodynamic therapy," *Chem. Commun.* **49**(79), 8934–8936 (2013).
17. J. R. Starkey et al., "New two-photon activated photodynamic therapy sensitizers induce xenograft tumor regressions after near-IR laser treatment through the body of the host mouse," *Clin. Cancer Res.* **14**(20), 6564–6573 (2008).
18. D. L. Sackett, "Podophyllotoxin, steganacin and combretastatin; natural products that bind at the colchicine site of tubulin," *Pharm. Ther.* **59**(2), 163–228 (1993).
19. J. A. Hadfield et al., "Tubulin and microtubules as targets for anticancer drugs," *Prog. Cell Cycle Res.* **5**, 309–325 (2003).
20. G. C. Tron et al., "Medicinal chemistry of combretastatin A4: present and future directions," *J. Med. Chem.* **49**(11), 3033–3044 (2006).
21. J. H. Bilenker et al., "Phase I trial of combretastatin A-4 phosphate with carboplatin," *Clin. Cancer Res.* **11**(4), 1527–1533 (2005).
22. M. Zweifel et al., "Phase II trial of combretastatin A4 phosphate, carboplatin, and paclitaxel in patients with platinum-resistant ovarian cancer," *Ann. Oncol.* **22**(9), 2036–2041 (2011).
23. R. H. Bisby et al., "Fluorescence lifetime imaging of E-combretastatin uptake and distribution in live mammalian cells," *Eur. J. Cancer* **48**(12), 1896–1903 (2012).
24. R. H. Bisby et al., "Time-resolved nanosecond fluorescence lifetime imaging and picosecond infrared spectroscopy of combretastatin A-4 in solution and in cellular systems," *Meas. Sci. Technol.* **23**(8), 084001 (2012).
25. K. M. Scherer et al., "An anticancer phototherapy using activation of E-combretastatins by two-photon induced isomerization," *J. Biomed. Opt.* **20**(5), 051004 (2015).
26. S. W. Botchway et al., "A series of flexible design adaptations to the Nikon E-C1 and E-C2 confocal microscope systems for UV, multiphoton and FLIM imaging," *J. Microsc.* **258**(1), 68–78 (2015).
27. E. Fennema et al., "Spheroid culture as a tool for creating 3D complex tissues," *Trends Biotechnol.* **31**(2), 108–115 (2013).
28. P. Indovina et al., "Three-dimensional cell organization leads to almost immediate HRE activity as demonstrated by molecular imaging of MG-63 spheroids using two-photon excitation microscopy," *FEBS Lett.* **581**(4), 719–726 (2007).
29. H. Ma et al., "Multicellular tumor spheroids as an *in vivo*-like tumor model for three-dimensional imaging of chemotherapeutic and nano material cellular penetration," *Mol. Imaging* **11**(6), 487–498 (2012).
30. M. D. Bregman and F. L. Meyskens, "In vitro modulation of human and murine melanoma growth by prostanoid analogues," *Prostaglandins* **26**(3), 449–456 (1983).
31. L. le Roux et al., "Optimizing imaging of three-dimensional multicellular tumor spheroids with fluorescent reporter proteins using confocal microscopy," *Mol. Imaging* **7**(5), 214–221 (2008).
32. R. H. Bisby and E. W. Thomas, "Kinetic analysis by the method of non-linear least squares: a reaction involving consecutive steps," *J. Chem. Educ.* **63**(11), 990–992 (1986).
33. K. M. Scherer et al., "Spectroscopy and fluorescence lifetime imaging in live cells of a cyano-substituted combretastatin," *Biomed. Spectrosc. Imaging* **3**(3), 211–218 (2014).
34. K. M. Scherer, "Two-photon microscopy of E-combretastatin uptake and activation in live mammalian cells," PhD Thesis, University of Salford (2012).
35. H. W. Ma et al., "A dual functional fluorescent probe for glioma imaging mediated by blood-brain barrier penetration and glioma cell targeting," *Biochem. Biophys. Res. Commun.* **449**(1), 44–48 (2014).
36. H. L. Wong et al., "Paclitaxel tumor-priming enhances siRNA delivery and transfection in 3-dimensional tumor cultures," *Mol. Pharm.* **8**(3), 833–840 (2011).
37. F. Pampaloni, N. Ansari, and E. H. K. Stelzer, "High-resolution deep imaging of cellular spheroids with light-sheet-based fluorescence microscopy," *Cell Tissue Res.* **352**(1), 161–177 (2013).
38. T. H. Foster et al., "Fluence rate effects in photodynamic therapy of multicell tumor spheroids," *Cancer Res.* **53**(6), 1249–1254 (1993).
39. C. L. Evans et al., "Killing hypoxic cell populations in a 3D tumor model with EtNBS-PDT," *PLoS ONE* **6**(8), e23434 (2011).
40. J. P. Celli et al., "An imaging-based platform for high-content, quantitative evaluation of therapeutic response in 3D tumor models," *Sci. Rep.* **4**, 3751 (2014).
41. C. L. Evans, "Three-dimensional *in vitro* cancer spheroid models for photodynamic therapy: strengths and opportunities," *Front. Phys.* **3**(15), article 15 (2015).
42. A. Nanashima et al., "How to access photodynamic therapy for bile duct carcinoma," *Ann. Transl. Med.* **2**(3), 23 (2014).
43. Y. Y. Huang et al., "Melanoma resistance to photodynamic therapy: new insights," *Biol. Chem.* **394**(2), 239–250 (2013).
44. A. Hollebecque, C. Massard, and J.-C. Soria, "Vascular disrupting agents: a delicate balance between efficacy and side effects," *Curr. Opin. Oncol.* **24**(3), 305–315 (2012).

**Kathrin M. Scherer** received her BSc and PhD degrees from the University of Salford in 2009 and 2013. Since November 2012, she has been a postdoctoral researcher within the Central Laser Facility at the Rutherford Appleton Laboratory STFC, using advanced fluorescence imaging techniques including confocal multiphoton fluorescence lifetime microscopy (FLIM), single-molecule TIRF, and super-resolution STED microscopy to study biomedically relevant processes. She has authored seven peer-reviewed publications and has one patent.

**Roger H. Bisby** received his BSc and PhD degrees from the University of Nottingham in 1969 and 1973. He is an emeritus professor at the University of Salford and a fellow of the Royal Society of Chemistry. He has authored over 90 scientific publications that reflect his lifelong interest in fast reactions and biochemical spectroscopy.

**Stanley W. Botchway** his BSc (chemistry 1990) and PhD (1996) from the University of Leicester followed by a fellowship at Harvard Medical School. Currently, he is a visiting professor at Oxford Brookes University and an STFC senior scientist. He has developed laser applications including instruments for ultrafast microbeam irradiation of cellular DNA and multiphoton FLIM. He has authored over 70 papers and is a member of the Royal Society of Chemistry and Radiation Research Society.

**John A. Hadfield** is a senior lecturer in medicinal chemistry at the University of Salford. He received his BSc degree in chemistry from the University of Nottingham in 1979 and his PhD in organic chemistry from Trent Polytechnic in 1984. He is the author of more than 50 journal papers and was chairman of Onco-NX (2011 to 2014). His research interests include the development of anticancer drugs, especially antivasculature agents.

**John W. Haycock** received his BSc and PhD degrees in biochemistry from the University of Newcastle followed by a Fellowship at Albany Medical College, New York, in 1991 and 1994. Currently, he is professor of bioengineering at the University of Sheffield. He has authored more than 100 publications on soft tissue regeneration and the development of reconstructed and preclinical models of nerve and skin for experimental and translatable purposes.

**Anthony W. Parker** received his PhD (University of Warwick, photochemistry of DNA) and was postdoctoral fellow at the Royal Institution (Great Britain). He joined the Rutherford Appleton Laboratory in 1986. He is now STFC fellow applying Raman spectroscopy to bone disease, coinventor of Spatially Offset Raman Spectroscopy with 5 patents and 250 publications. He has honorary chairs at UCL and Universities of Salford and Stellenbosch and is a fellow of the Royal Society of Chemistry.